Ball, M. W. Fanger, S. Hakomori, V. Ginsburg, *Arch. Biochem. Biophys.* **233**, 501 (1984).
10. H. C. Gooi *et al.*, *Eur. J. Immunol.* **13**, 306 (1983); P. A. T. Tetteroo *et al.*, *ibid.* **14**, 1089 (1984).
11. F. W. Symington, I. D. Bernstein, S. Hakomori, *J. Biol. Chem.* **259**, 6008 (1984).
12. B. A. Macher, J. Buehler, P. Scudder, W. Knapp, T. Feizi, *ibid.* **263**, 10186 (1988).
13. P. Fredman *et al.*, *Biochem.* **251**, 17 (1988).
14. K. Fukushima *et al.*, *Cancer Res.* **44**, 5279 (1984).
15. M. Fukuda, E. Spooncer, J. E. Oates, A. Dell, J. C. Klock, *J. Biol. Chem.* **259**, 10925 (1984); E. Spooncer, M. Fukuda, J. C. Klock, J. E. Oates, A. Dell, *ibid.* **259**, 4792 (1984); Y. Fukushi, E. Nudelman, S. B. Levery, S. Hakomori, H. Rauvala, *ibid.* **259**, 10511 (1984); Y. Fukushi *et al.*, *Cancer Res.* **45**, 3711 (1985).
16. F.-G. Hanisch, G. Uhlenbruck, J. Peter-Katalinck, H. Egge, *Carbohydr. Res.* **178**, 29 (1988).
17. D. Biou *et al.*, *Biochim. Biophys. Acta* **913**, 308 (1987); J. M. Wieruszeski, B. Fournet, D. Konan, D. Biou, G. Durand, *FEBS Lett.* **238**, 390 (1988).
18. B. Fournet *et al.*, *Biochemistry* **17**, 5206 (1978).
19. F.-G. Hanisch, A. Mitsakos, H. Schroten, G. Uhlenbruck, *Carbohydr. Res.* **178**, 23 (1988); A. Mitsakos, F.-G. Hanisch, G. Uhlenbruck, *Biol. Chem. Hoppe Seyler* **369**, 661 (1988).
20. A. Mitsakos and F.-G. Hanisch, *Biol. Chem. Hoppe Seyler* **370**, 239 (1989).
21. More ELAM-Rg bound to plastic adsorbed with reaction mixture without DGP-fucose than to α_1-AGP alone, indicating that the removal of mucins (to which the enzyme binds tightly) (*8*) from the enzyme was incomplete.
22. M. A. Gimbrone, Jr., *et al.*, *Science* **246**, 1601 (1989).
23. K. M. Skubitz and R. W. Snook, *J. Immunol.* **139**, 1631 (1987); M. Albrechtsen and M. A. Kerr, *Br. J. Haematol.* **72**, 312 (1989).
24. K. D. Forsythe, A. C. Simpson, R. J. Levinsky, *Eur. J. Immunol.* **19**, 1331 (1989).
25. G. E. Rice and M. P. Bevilacqua, *Science* **246**, 1303 (1989). The WiDr cell line used in the present work is now known (*26*) to be derived from the HT-29 line used in the studies of Rice and Bevilacqua.
26. T. R. Chen, D. Drabkowski, R. J. Hay, M. Macy, W. Peterson, Jr., *Cancer. Genet. Cytogenet.* **27**, 125 (1987).
27. J. G. Bolscher *et al.*, *Clin. Exp. Metastasis* **7**, 557 (1989).
28. A. Aruffo and B. Seed, *EMBO J.* **6**, 3313 (1987a).
29. E. D. Ball, R. F. Graziano, M. W. Fanger, *J. Immunol.* **130**, 2937 (1983).
30. We thank P. Terasaki for donation of MAb CSLEX1, O. Majdic and W. Knapp for MAb VIM-2, I. Bernstein for MAb T5A7, and P. Fredman for MAb SulphI; R. Larsen and L. Hefner for samples of amniotic fluid; J. M. Kim for technical assistance; and members of the laboratory for discussion and advice. Supported by an American Society of Transplant Physicians Fellowship (G.W.), a Leukemia Society of America Fellowship (A.A.), a Pew Foundation Scholar in the Biomedical Sciences award (M.B.), NIH grants AI27849 and DK43031 (B.S.), HL36028 (M.P.B.), and by an award to the Massachusetts General Hospital from Hoechst AG.

30 August 1990; accepted 19 October 1990

The Enzymic Nature of Antibody Catalysis: Development of Multistep Kinetic Processing

STEPHEN J. BENKOVIC,* JOSEPH A. ADAMS, C. L. BORDERS, JR., KIM D. JANDA, RICHARD A. LERNER

Detailed kinetic investigations of a catalytic antibody that promotes the hydrolyses of an anilide and phenyl ester show that this catalyst uses a multistep kinetic sequence resembling that found in serine proteases to hydrolyze its substrates, although antibody was elicited to a single transition-state analog. Like the serine proteases the antibody catalyzes the hydrolysis reactions through a putative covalent intermediate, but unlike the enzymes it may use hydroxide ion to cleave the intermediates. Nevertheless, the antibody is a potent catalyst with turnover at higher pH values rivaling that of chymotrypsin. This analysis also reveals that turnover by the antibody is ultimately limited by product desorption, suggesting that improvements in catalytic efficiency may be achieved by judicious changes in the structure of the substrate, so that it is not superimposable on that of the eliciting hapten.

A VARIETY OF REACTIONS HAVE NOW been catalyzed by antibodies elicited to transition-state analogs and include a number of important reaction types (*1, 2*). These catalysts resemble enzymes in their mode of action, since substrate transformation is achieved through a preliminary binding event that generates a reactive antibody-substrate complex that in turn dissociates to products. Thus comparisons between appropriate enzyme-antibody pairs have been made, but these are based primarily on steady-state Michaelis-Menten parameters. We report the detailed description of the kinetic sequence of an antibody, NPN43C9, that catalyzes the hydrolysis of an aromatic amide as well as the corresponding aromatic ester (*3*). The resemblance of the number and mechanistic nature of the steps in this pathway to those of the serine proteases informs an analysis of the catalytic characteristics of this antibody relative to chymotrypsin. The appearance of a multistep kinetic sequence limited for the ester by-product desorption emphasizes an adaptive advantage of the esterase enzyme over the abzyme and identifies structural features of the eliciting transition-state analog that may be modified for catalytic advantage.

The antibody-catalyzed hydrolysis of the *p*-nitrophenyl ester **1** and *p*-nitroanilide **2** have been examined by both pre- and steady-state kinetic techniques. The steady-state Michaelis-Menten parameters, k_{cat}/K_M and k_{cat}, as a function of pH are displayed in Fig. 1. The data can be fit either to a reaction mechanism involving the titration of a group at the antibody binding site whose dissociation promotes substrate hydrolysis or to one that features a change in the rate-limiting step around an intermediate antibody-bound species due to changes in pH (*4*). An examination of the rates of product release from the antibody (Table 1), measured by stopped-flow competition experiments monitoring the increase in antibody fluorescence (340 nm) upon dissociation of the product molecule, revealed that the rate constants for product dissociation are the parent acid >*p*-nitroaniline (PNA) >*p*-nitrophenol (PNP), suggesting that the nitro residue is a major determinant of antigen binding. Moreover, the rate constant for PNP release ($45 \pm 10\ s^{-1}$) sets the maximum value of k_{cat} ($40 \pm 6\ s^{-1}$) for ester hydrolysis (the pH-independent region, pH > 9 in Fig. 1). (Error limits are ± SE throughout.) Thus, the antibody-catalyzed hydrolysis of **1** proceeds through at least two steps whose relative importance in determining the rate of a reaction cycle change with pH. The identification of k_{cat} (pH > 9) with the rate constant for *p*-nitrophenolate release and the 10^4 difference in k_{cat} values (pH > 9) for **1** and **2** moreover eliminate a mechanism involving productive

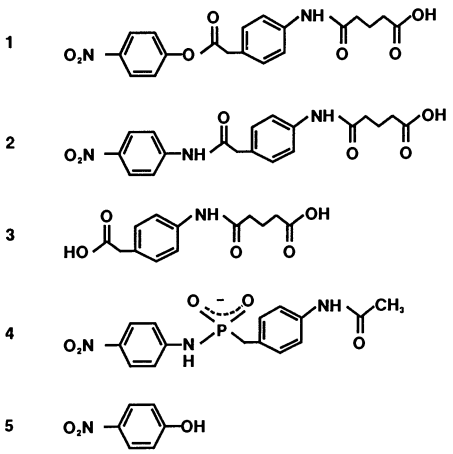

S. J. Benkovic and J. A. Adams, Pennsylvania State University, Department of Chemistry, University Park, PA 16802.
C. L. Borders, Jr., The College of Wooster, Department of Chemistry, Wooster, OH 44691.
K. D. Janda and R. A. Lerner, Scripps Clinic and Research Foundation, La Jolla, CA 92037.

*To whom correspondence should be addressed.

Table 1. Rate constants for product dissociation from NPN43C9(Ab); PNA, and PNP. Thermodynamic dissociation constants (K_d) were measured from the ligand-dependent quenching of the intrinsic antibody fluorescence on an SLM 8000 spectrofluorimeter. The observed intensity was corrected for inner-filter absorbance effects by titrating a known tryptophan solution side by side with the antibody and fitting the data to a quadratic solution (*27*). Dissociation rate constants (k_{off}) were measured by monitoring the time-dependent change in fluorescence upon substitution of the bound ligand with the transition-state 4 analog in a stopped-flow spectrofluorimeter; k_{off} for PNA was measured by competing with PNP. All competition experiments were performed in ATC buffer at 25°C. The K_d values for the ligands were measured in ATE buffer at 25°C, pH 7.0.

Ligand	Complex	K_d(μM)	k_{off} (s^{-1})	
			pH 7	pH 10
Acid **3**	Ab · **3**	28 ± 5	330 ± 40	
PNA	Ab · PNA	9.3 ± 1.6		500 ± 50
PNP	Ab · **5**	1.0 ± 0.2	43 ± 6	45 ± 10

and unproductive binding of substrate to antibody as responsible for the abrupt change in slope in the two pH-k_{cat} profiles, since such a sequence would require similar values of k_{cat} above pH 9 for both substrates (*5*).

Direct stopped-flow measurements of the rates of PNP binding to NPN43C9 through fluorescent quenching of intrinsic antibody fluorescence (290-nm excitation, 340-nm emission) gave rate constants linearly proportional to ligand concentration, which suggests simple one-step binding of the reagent to the antibody. At pH 6.0, the rate of PNP association with NPN43C9 also can be obtained by monitoring the increase in absorbance at 404 nm arising from the partial conversion of PNP to the phenolate upon forming the binary complex (Fig. 2). The linear dependence of the observed rate constants derived from such transients on [PNP] gave a pseudo–first-order rate constant (k_{on}) for association of the ligand with the antibody of 46 ± 1 μM^{-1} s^{-1} at pH 6.0. The satisfactory correspondence between the direct thermodynamic measurement of *p*-nitrophenolate dissociation from NPN43C9 (K_D = 1.0 μM) and that calculated from the ratio of rate constants (k_{off}/k_{on} = 1.0 μM) is in accord with the one-step binding scheme.

Reaction of the antibody with PNP in the presence of the phosphonamide transition-state analog **4** (used to induce NPN43C9) showed that both compete for a common binding site owing to the decrease in the relative amplitude of the absorbance increase (insert, Fig. 2) when **4** was present. Since the K_D for **4** (measured by titrating with **4** the intrinsic antibody fluorescence) is ~0.8 ± 0.2 nM, the data were linearly extrapolated to higher ratios of [**4**]/[NPN43C9] to implicate a 2:1 PNP:antibody stoichiometry, which reflects the homogeneity of the protein preparation.

The calculated amplitude of 0.9 ± 0.1 equivalents of PNP bound per two equivalents of antibody (Fig. 2) is one-half of the quantity expected from the total occupancy of both sites. This discrepancy may be rationalized by having bound equal concentrations of *p*-nitrophenolate and PNP (nonabsorbing at 404 nm) to the antibody at pH 6.0. The solution pK_a of PNP then is reduced from ~7.1 to ~6.0, suggesting the presence of an electropositive environment that stabilizes the oxyanion of *p*-nitrophenolate and probably contributes to the slow k_{off} for this ligand.

Evidence for or against the accumulation of an intermediate in the chemical step, such as an acyl antibody derived from covalent attachment of the acyl moiety of **3** to a nucleophilic side chain in the binding site, was sought in several types of experiments. A simple hydrolytic mechanism would, of course, require no covalent intermediate but should feature general acid-base catalysis of ester **1** or particularly amide **2** hydrolysis. Measurement of the pH-k_{cat} and k_{cat}/K_M profiles for the hydrolysis of **2** in D_2O revealed no evidence for a deuterium solvent isotope effect characteristic of this type of mechanism (*6*). This evidence, in conjunction with the slow product release noted for ester hydrolysis, eliminates a mechanism in which a dissociable group on the antibody catalyzes substrate hydrolysis in a rate-limiting chemical step.

In light of these results, clues were sought for the presence of an intermediate. In one experiment the antibody-catalyzed hydrolysis of *p*-nitrophenyl ester **1** was followed by rapidly quenching the reaction at pH 7.0 with 0.2 M formic acid. Control experiments showed negligible spontaneous hydrolysis of the ester under these conditions. Determination by high-performance liquid chromatography (HPLC) of the amounts of acid **3** and PNP produced as a function of time (Fig. 3) revealed no rapid initial formation of either product, with both being coproduced at the same rate with the expected 1:1 stoichiometry. In a related experiment stopped-flow detection of *p*-nitrophenolate release at 350 nm (the isobestic wavelength where the absorbance of the acid and base species of the phenol is equal) (*7*) in the presence of 4 μM concentrations of NPN43C9 and 200 μM ester did not reveal rapid biphasic liberation of PNP (Fig. 4). These two experiments exclude the rapid formation of an intermediate that accumulates to greater than ~5% of the antibody concentration (our level of detection), but of course do not exclude the possibility of such a species being present at steady-state levels. The pH independence of K_M values for both anilide and ester required by the similar pH dependence in k_{cat} and k_{cat}/K_M also rules against the interpretation that the changes in slope in the pH-rate profiles are

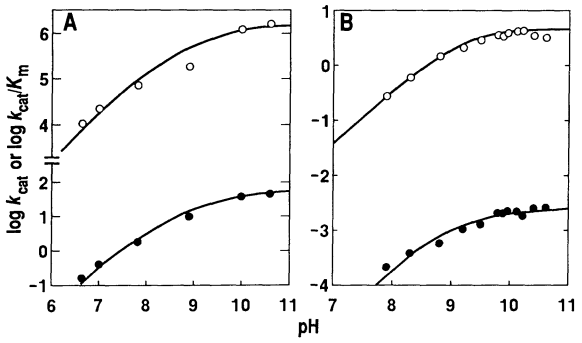

Fig. 1. The pH-dependent steady-state kinetics for (**A**) the ester reaction were done by mixing equal volumes of ester in 5 mM Aces (pH 4) and antibody in 2× ATC buffer (final buffer concentrations: 100 mM Aces, 50 mM tris, 50 mM Caps) at the desired pH in a stopped-flow spectrophotometer (designed by K. Johnson) and observing absorbance changes at 404 nm. No significant pH changes were observed upon mixing (≤0.2 units over a pH range of 6.6 to 10.8). An extinction coefficient ε of 23,100 M^{-1} for the ionized phenol at this path length was measured by converting known amounts of the ester to products with 0.1 M KOH in the stopped-flow apparatus. Ester reactions were run at 25°C with 2.5% (v/v) dioxane for substrate solubilization. Calculated lines fitted to pK_a = 9.1 ± 0.1 (k_{cat}, ●); pK_a = 8.9 ± 0.1 (k_{cat}/K_M, ○) with an equation of the form log y = log [$C/(1 + H/K_a)$], where y and C are, respectively, the pH-dependent and pH-independent values of k_{cat} or k_{cat}/K_M. The pH-dependent steady-state parameters for (**B**) the amide reaction were measured by manual mixing of antibody and amide and observing absorbance changes at 404 nm in ATE (100 mM Aces, 52 mM tris, 52 mM ethanolanine) buffer at 37°C, 5% dimethylformamide v/v. An extinction coefficient of 10,700 M^{-1} was used for the quantification of *p*-nitroaniline. Calculated lines fitted to pK_a = 9.0 ± 0.1 (k_{cat}, ●); pK_a = 9.1 ± 0.1 (k_{cat}/K_M, ○). The antibody concentrations for ester and amide reactions were determined by direct titration of antibody with the transition-state analog **4** and a BCA (bicinchoninic acid) assay or both. Both methods gave equivalent results (Fig. 2).

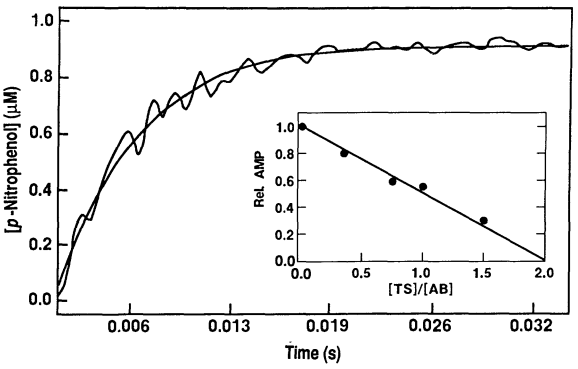

Fig. 2. Time-dependent increase in antibody-bound *p*-nitrophenolate as measured in a stopped-flow apparatus manufactured by Applied Photophysics (404 nm) at pH 6. For this transient, 4 μM PNP was rapidly mixed with 0.65 μM antibody (final concentrations). The bound PNP was quantitated from ε for the ionized species, 13,200 M^{-1} (404 nm) at this path length, presuming no change in ε upon binding. The antibody concentration is based on a molecular weight of 150,000. The relative amplitude for the binding of 4 μM PNP and 1 μM antibody as a function of the ratio of the transition-state analog to antibody is shown in the insert. A stoichiometry of 2.1 ± 0.1 molecules of PNP per antibody molecule is derived from the abscissa intercept. All experiments were done in ATC buffer, pH 6.0, 25°C.

due to the significant accumulation of an intermediate species (*8*).

The possibility that the reaction intermediate implicated by the pH-rate profiles is a tetrahedral species also must be entertained. A series of $H_2{}^{18}O$ experiments (*9*) for hydrolysis of *p*-nitroanilide **2** at pH 9.0 showed no ^{18}O exchange into remaining substrate (at ~40% reaction) and the expected incorporation of ^{18}O into the acid product (1.06 ^{18}O equivalents per equivalent of $H_2{}^{18}O$). From previous studies by Bender on a series of *p*-substituted acetanilides (*10*), one can estimate that the remaining substrate should have undergone nearly complete exchange (the ratio of the exchange to hydrolysis rates ~30) if the mechanism involved formation of a tetrahedral intermediate that lost OH^- randomly to reform **2**. The lack of ^{18}O exchange in the antibody-catalyzed hydrolysis of **2** would argue against the presence of a symmetrical tetrahedral intermediate (*11*) but not an asymmetric species within the binding site or a steady-state acyl-antibody species; both exclude the possibility of any amide-$H_2{}^{18}O$ exchange.

The two kinetic sequences proposed earlier with appropriate modification are consistent with the available kinetic data. The first in outline form features the reaction of the antibody with either substrate to form a putative acyl intermediate, which hydrolyzes through water attack (Scheme 1).

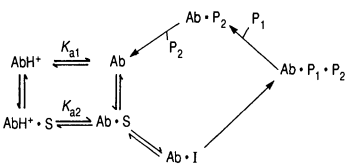

Scheme 1

The reactivity of the active site nucleophile is controlled by its pK_a in the uncomplexed and substrate complex ($pK_{a1} \approx pK_{a2}$ from Fig. 1). The second is given by the kinetic sequence displayed in Scheme 2 and likewise features formation of a putative acyl intermediate that deacylates, however, through OH^- attack. In this case the pK_a of the active site nucleophile is presumed to be outside our pH range of observation.

One means of distinguishing between these two alternatives is to demonstrate that the equilibrium binding of a competitive inhibitor is sensitive to the ionization state of an active site group (*12*). The binding of the *p*-nitroanilide **2**, as a competitive inhibitor of ester hydrolysis, is independent of pH (K_i = 260 ± 80 μM, pH 7.0; K_i = 190 ± 60 μM, pH 9.8); the binding of PNP as reflected in k_{off} is also pH independent (Table 1). In addition, the slow dissociation rate of PNP should in the case of ester hydrolysis perturb the pK_a observed in the k_{cat}-pH profile by ~0.7 units (*12*).

We then analyzed the kinetic data in terms of Scheme 2 (*13*). The relevant rate equations for this sequence are listed in (*14*). Since the terms k_4 and k_5, the dissociation rates of the various products, and the ratio of k_{-1}/k_1, the dissociation constant for substrate, have been determined, it is possible, in combination with the pH dependencies of k_{cat} and k_{cat}/K_M, to solve or estimate all of the rate coefficients associated with Scheme 2 for both **1** and **2**.

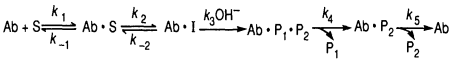

Scheme 2

Beginning with ester **1**, one may proceed through the analysis as follows. Since no rapid release of *p*-nitrophenolate from **1** was observed under pre–steady-state conditions, the equilibrium constant between Ab · S ⇌ Ab · I (k_2/k_{-2}) can be no greater than 1/20, presuming a detection limit of 5% product, so that $k_{-2} > k_2$. This step must be reversible; if not, k_{cat}/K_M would be pH independent. Secondly, the rate k_5 of release of *p*-nitrophenolate from (Ab · P_2) is 45 s^{-1} (at pH 10), a rate that approximates the value of k_{cat} at its plateau rate at high pH. As a consequence, k_{cat} (pH < 9.0) ≈ 9 $k_2k_3OH^-/k_{-2}$ and k_{cat} (pH > 9.0) ≈ 9 $k_2k_5/(k_2 + k_5)$, which accounts for the pH dependence in k_{cat}. Given the error estimates in k_{cat} (pH > 9.0) and k_5, the minimum value of k_2 or acylation is ≥ 180 s^{-1}. It follows from k_{cat} (pH < 9.0) and our above estimate of k_2/k_{-2} that $k_3 \geq 60$ μM^{-1} s^{-1} for OH^--catalyzed deacylation (*15*) and $k_{-2} \geq 3600$ s^{-1}. Finally, various combinations (*16*) of k_{cat} and k_{cat}/K_M can be used to solve for k_1 (1.3 μM^{-1} s^{-1}) and k_{-1} (25 ± 4 s^{-1}).

The pH-rate profile for k_{cat} is thus generated from a change in rate-limiting step from *p*-nitrophenolate release at high pH to OH^--mediated hydrolysis at low pH of Ab · I, assigned as a putative acylated antibody; for k_{cat}/K_M the profile likely describes a change from rate-limiting OH^--mediated

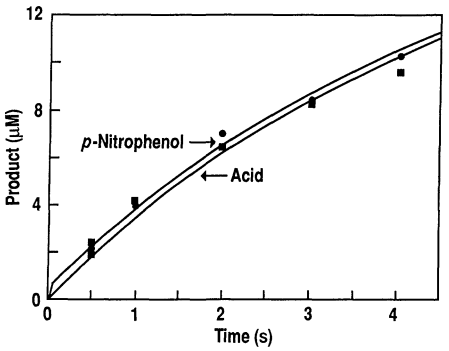

Fig. 3. The time-dependent production of the acid (●) and PNP (□) products was monitored by reversed-phase HPLC after the rapid quenching of the ester reaction in acid media at discrete time intervals. Antibody (26 μM) in 2× ATC (pH 7.0) was mixed with an equal volume of 400 μM ester in 5 mM formic acid (pH 3). Final reaction concentrations were 13 μM antibody and 200 μM ester. Following a desired mixing time (0.50 to 5.0 s), the reaction was quenched with 0.2 M formic acid. The quenched samples were immediately frozen and stored at −80°C until quantitative analysis was done by reversed-phase HPLC equipped with a Waters 600E controller, Waters 484 variable wavelength detector, and a Hewlett-Packard 3394A integrator. The products were separated with a Vydac C_{18} (4.6 cm by 25 cm) column and a programmed gradient of 0.1% trifluoroacetic acid–acetonitrile at a flow rate of 1.0 ml/min. Standard curves relating integrated peak area to the concentration of the product were generated with a detection wavelength of 265 nm for acid **3** and 305 nm for PNP. Two runs of each quenched sample were carried out, one at a detector setting of 265 nm and the other at 305 nm, and the concentration of each product was determined from the corresponding standard curve. Control quench solutions (without antibody) were generated for each mixing time and separated, and the data were used to correct the concentration of products in the runs containing antibody. The data were fit to Scheme 2 using the rate constants outlined in Fig. 5 with the kinetic simulation program KINSIM (*26*).

deacylation of the putative acylated antibody at low pH to diffusional control of antibody-substrate association at high pH.

The analysis of the kinetic sequence for the anilide is similar. The value of k_{-1}/k_1 is obtained directly as the pH-independent K_M, or K_i for competitive inhibition of ester hydrolysis by the anilide (*17*). However, the term k_{cat} (pH > 9.0) does not equate with any product-dissociation step (Table 1), so that this pH-independent rate is assigned to the putative acylation step k_2. The low magnitude of the rate for this step permits substrate binding to antibody to be at equilibrium. Since the deacylation step likely involves hydrolysis of a common acyl intermediate—ignoring the possible influence of P_2—its value is left unchanged. The evaluation of $k_{-2} \geq 630\ s^{-1}$ stems from solving by substitution into the expression for k_{cat} (pH < 9.0) (*18*). Thus, the pH-rate profiles for both k_{cat} and k_{cat}/K_M represent a change from rate-limiting OH^--mediated hydrolysis of the acylated antibody at low pH to its acylation at high pH (*19*).

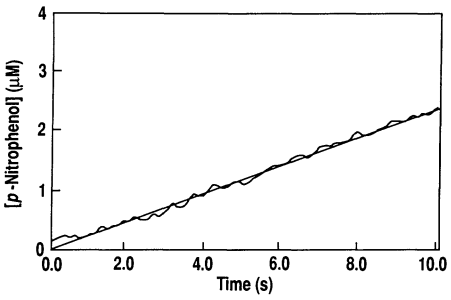

Fig. 4. The production of *p*-nitrophenol for the ester reaction as a function of time at pH 6. Antibody (4 μM final concentration) was mixed with ester (200 μM final concentration) in an Applied Photophysics stopped-flow spectrophotometer. Increases in PNP–*p*-nitrophenolate were monitored at an isobestic wavelength (350 nm) with an extinction coefficient of 3600 M^{-1}. The data were fit to a line of slope 0.2 μM/s (k_{obs} = 0.05 s^{-1}). The ordinate axis is corrected for the linear, background hydrolysis of the ester. Transients collected over a 50-ms time range gave a similar slope as that for the 10-s trace. All stopped-flow experiments were performed at 25°C in ATC buffer containing 2.5% dioxane without low-pH preequilibration of the substrate.

The relative importance of the various kinetic steps in antibody turnover of the two substrates can be more easily visualized through the aid of a free-energy (ΔG) reaction-coordinate diagram (Fig. 5). There are several striking features of the two reaction profiles. One is the high stability of the $Ab \cdot P_1 \cdot P_2$ product complex, which has a ΔG 7 to 12 kcal/mol lower than the respective uncomplexed substrates. This tight product complex ultimately limits the rate of product dissociation in the hydrolysis of the ester. A second feature is the increased kinetic barrier for formation of Ab · I from the amide relative to the ester substrate, so that this step eventually limits amide turnover by the antibody. The ratio of rate constants for this step for the ester and amide substrates is $\geq 8 \times 10^4$; for comparison, the ratio of the rates of acylation of chymotrypsin by *N*-acetyl-L-Phe *p*-nitrophenyl ester and *N*-acetyl-L-Tyr-*p*-nitroanilide is $\sim 4 \times 10^5$. The individual comparable rate constants for acylation by the enzyme are 23,700 and 0.05 s^{-1}, some 130- to 25-fold faster than the corresponding steps for antibody (*20, 21*). This loose analogy should not be construed to mean that a serine is the actual nucleophile used by NPN43C9; the identity of this residue remains to be ascertained, but whatever the nature of this residue it does not dissociate over the pH range used. The differences in the k_{-2} step for ester and anilide (greater than sixfold) is also the expected reactivity pattern for *p*-nitrophenolate and anilide nucleophiles with activated esters and amides (*22*). Finally, we note that the serine proteases catalyze their deacylation through a general acid-base mechanism, while in the antibody solvent apparently furnishes the requisite OH^- species directly. Nevertheless, the pathways used by NPN43C9 and a serine protease bear a remarkable resemblance; both use a series of steps around an isoenergetic intermediate to achieve ester or amide cleavage (*23, 24*).

The ΔG profile of Fig. 5 in some ways is a view of how primitive, non-optimized enzymes may have functioned. The efficiency of turnover is hampered by the unevenness in the ΔG barriers for the various internal antibody-substrate states and their respective transition states. A more optimal situation would balance the differences in ΔG between the external and internal ground states and their respective transition states so that no single ΔG barrier would be egregious (*25*). Despite its limitations, NPN43C9 is a potent catalyst, with k_{cat} values at pH > 9.0 that are roughly within a factor of 25 of chymotrypsin at pH 7.0 (*20, 21*). For the chymotrypsin-catalyzed hydrolysis of *N*-acetyl-L-Phe *p*-nitrophenyl ester, k_{cat} is 77 s^{-1}, while for *N*-acetyl-L-Tyr-*p*-nitroanilide, k_{cat} is 0.051 s^{-1}; for the NPN43C9-catalyzed hydrolysis of **1**, k_{cat} is 40 s^{-1}, while for **2**, k_{cat} is 0.002 s^{-1} (at 37°C). The means to further improve the catalytic efficiency of antibodies must be gained by: (i) the introduction of additional catalytic residues to provide the opportunity for multifunctional catalysis; and (ii) the use of substrates that do not retain all of the prominent structural features of the inducing transition-state analog in order to avoid too tight binding of products.

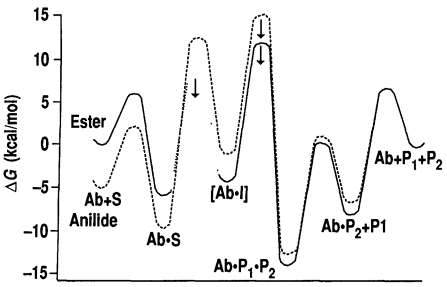

Fig. 5. Reaction ΔG profile for antibody-catalyzed ester (—) and anilide (---) hydrolysis at pH 7. The association rate constant for PNP binding (P_2) was measured directly (Fig. 2; 46 μM^{-1} s^{-1}), while that for the ester (S) was deduced from k_{cat}/K_M at high pH (1.3 μM^{-1} s^{-1}). The association rate constants for the acid (P_1) and PNA (P_2) were set equal to that of PNP (46 $\mu M^{-1} s^{-1}$), while that for the anilide (S) was equated with the ester. The dissociation rate constants for PNP, PNA, and acid were measured directly from competition experiments (Table 1), while that for the ester was deduced from steady-state kinetics (see text). The K_d for the anilide was obtained from K_M [see text and (*17*)]. For the anilide the forward rate constant for intermediate formation (k_2) was measured directly from k_{cat} at high pH (0.0022 s^{-1}), whereas for the ester the lower limit for k_2 was deduced from steady-state constraints ($\geq$180 s^{-1}; see text). The uncertainty in this step for the ester hydrolysis is highlighted by the dotted line. Values for k_{-2} ($\geq$3600 s^{-1} and $\geq$630 s^{-1}) for **1** and **2** were set by k_{cat} (< pH 9.0) assuming a maximum ratio of $k_2/k_{-2} \approx 0.05$ for **1** and a common first-order rate constant (k_3) of 60 μM^{-1} s^{-1}. The ground-state energy of the anilide was set 5 kcal/mol lower than the arbitrarily fixed value for the ester (*24*). The free-product ground-state energies for protonated acid and neutral *p*-nitrophenol and *p*-nitroaniline were fixed at 0 kcal/mol (*24*) and were not corrected to pH 7. The standard states of all substrate and products are 1 M.

REFERENCES AND NOTES

1. R. A. Lerner and S. J. Benkovic, *Chemtracts Org. Chem.* **3**, 1 (1990).
2. P. Schultz, R. A. Lerner, S. J. Benkovic, *Chem. Eng. News* **68** (no. 22), 26 (1990).
3. K. D. Janda, D. Schloeder, S. J. Benkovic, R. A. Lerner, *Science* **241**, 1188 (1988).
4. A. Fersht, *Enzyme Structure and Mechanism* (Freeman, San Francisco, 1977), chap. 5.
5. A simple sequence involving OH^--mediated hydrolysis of productively bound substrate, Ab_aS, in equilibrium with an unproductive species, Ab_iS, for example

$$Ab_iS \underset{k_{-c}}{\overset{k_c}{\rightleftharpoons}} Ab_aS \overset{k_{OH^-}}{\rightarrow} Ab + P_1 + P_2$$

can be used to generate the required pH-dependence in k_{cat}. At high pH, the rate of conformational change k_c would become rate limiting. Given the close structural similarities between the two substrates, however, one would expect the values of k_{cat} (pH > 9) to be similar, contrary to what is observed.
6. T. C. Bruice and S. J. Benkovic, *Bioorganic Mechanisms* (Benjamin, New York, 1966), vol. 1, chap. 1.
7. The use of the isobestic wavelength eliminates the possibility of an experimental artifact caused by PNP contamination in the ester that would produce a rapid increase in absorbance upon binding and

dissociating to the phenolate at the antibody combining site.
8. A. R. Fersht and Y. Requena, *J. Am. Chem. Soc.* **90**, 7079 (1971).
9. K. D. Janda *et al.*, *ibid.*, in press.
10. M. L. Bender and R. J. Thomas, *ibid.* **83**, 4183 (1961).
11. J. K. Kirsch and E. Katchalski, *Biochemistry* **4**, 884 (1965).
12. W. W. Cleland, *Adv. Enzymol. Relat. Areas Mol. Biol.* **45**, 273 (1977).
13. The two schemes are not mutually exclusive, but at present there is no evidence for two apparent ionizations in the pH-rate profiles.
14.

$$k_{cat} = \frac{k_2k_3k_4k_5OH^-}{k_3OH^-[k_4k_5 + k_2(k_4 + k_5)] + k_4k_5(k_2 + k_{-2})}$$

$$k_{cat}/K_M = \frac{k_1k_2k_3OH^-}{k_3OH^-(k_2 + k_{-1}) + k_{-1}k_{-2}}$$

$$K_M = \frac{[k_3OH^-(k_2 + K_{-1}) + k_{-1}k_{-2}]k_4k_5}{k_1[k_3OH^-(k_4k_5 + k_2k_4 + k_2k_5) + k_4k_5(k_2 + k_{-2})]}$$

At low pH the equations reduce to:

$$k_{cat}(pH < 9.0) \approx \frac{k_2k_3OH^-}{k_2 + k_{-2}}$$

$$k_{cat}/K_M(pH < 9.0) \approx \frac{k_1k_2k_3OH^-}{k_{-1}k_{-2}}$$

At high pH the equations reduce to:

$$k_{cat}(pH > 9.0) \approx \frac{k_2k_4k_5}{k_4k_5 + k_2(k_4 + k_5)}$$

$$k_{cat}/K_M(pH < 9.0) \approx \frac{k_1k_2}{k_2 + k_{-1}}$$

15. The large value for k_3 implies that deacylation may occur through a bound OH^- species.
16. The product of k_{cat} (pH < 9.0) times k_{cat}/K_M (pH < 9.0) divided by k_{cat}/K_M (pH < 9.0) equals $k_{-1}k_2/(k_2 + k_{-1})$ and can be used to evaluate k_{-1}. The term k_{cat}/K_M (pH > 9.0) then can be used to obtain k_1. Similar checks on the internal consistency of the numerical solutions are obtained by evaluating K_M at both extremes of pH, yielding a range from 19 to 30 μM. The experimentally determined values of K_M are 15 μM (pH 6.6) and 40 μM (pH 10).
17. The values of K_M and K_i are the same, within experimental error, under a wide range of experimental conditions: K_M = 180 ± 20 μM, ATE buffer, pH 9.0, 37°C; K_i = 260 ± 80 μM, 50 mM Pipes, 5% dioxane v/v, pH 7.0, 25°C; K_i = 190 ± 60 μM, ATC, 2.5% dioxane v/v, pH 9.8, 25°C.
18. Various checks of the kinetic data for internal consistency show, for example, that as required k_{cat} (pH < 9.0)/k_{cat} (pH > 9.0) ≈ k_{cat}/K_M (pH 9.0)/ k_{cat}/K_M (pH < 9.0); k_{cat} (pH < 9.0) divided by k_{cat}/K_M (pH < 9.0) ≈ K_M.
19. It can be shown from the pairs of equations for k_{cat} and k_{cat}/K_M that the apparent pK_a values in the k_{cat} and k_{cat}/K_M profiles for the amide **2** must be equal; for the ester **1** the same is true when $k_{-1} \approx k_5$.
20. B. Zerner, R. P. M. Bond, M. L. Bender, *J. Am. Chem. Soc.* **86**, 3674 (1964).
21. T. Inagami, A. Patchornik, S. S. York, *J. Biochem. (Tokyo)* **65**, 809 (1969).
22. W. P. Jencks and M. Gilchrist, *J. Am. Chem. Soc.* **90**, 2622 (1968).
23. M. L. Bender and F. J. Kezdy, *ibid.* **86**, 3704 (1964).
24. M. L. Bender *et al.*, *ibid.*, p. 3714.
25. W. J. Albery and J. R. Knowles, *Biochemistry* **15**, 5631 (1976).
26. B. A. Barshop, R. F. Wren, C. Frieden, *Anal. Biochem.* **130**, 134 (1983).
27. S. R. Stone and J. F. Morrison, *Biochemistry* **23**, 2753 (1984).
28. Supported in part by an NIH grant GM4385801 to K.D.J. C.L.B. was on research leave from The College of Wooster, Wooster, Ohio, during 1989–1990. We thank M. I. Weinhouse, J. A. Ashley, D. A. Mcleod, and D. M. Schloeder for expert technical assistance.

11 June 1990; accepted 10 September 1990

Dissociation of gp120 from HIV-1 Virions Induced by Soluble CD4

JOHN P. MOORE,* JANE A. MCKEATING, ROBIN A. WEISS, QUENTIN J. SATTENTAU

The CD4 antigen is the high affinity cellular receptor for the human immunodeficiency virus type–1 (HIV-1). Binding of recombinant soluble CD4 (sCD4) or the purified V1 domain of sCD4 to the surface glycoprotein gp120 on virions resulted in rapid dissociation of gp120 from its complex with the transmembrane glycoprotein gp41. This may represent the initial stage in virus-cell and cell-cell fusion. Shedding of gp120 from virions induced by sCD4 may also contribute to the mechanism by which these soluble receptor molecules neutralize HIV-1.

IN THE PREDOMINANT ROUTE OF HIV-1 infection, the virus binds to the cell surface via a high affinity interaction between gp120 and the cellular protein CD4 (*1, 2*). The gp120 protein is held on the virion surface by a noncovalent interaction with gp41 (*3*). Thus, the initial complex between virus and cell comprises gp41-gp120-CD4. Subsequently, pH-independent fusion of the cellular and viral membranes takes place, which allows entry of the viral genome into the cytoplasm (*4*). A similar process probably occurs during the fusion of gp120-gp41–expressing infected cells with CD4-expressing uninfected cells. The precise mechanism by which fusion takes place is unknown (*5*), but the fusigenic domain of the virus has been mapped to the hydrophobic NH_2-terminus of gp41 (*6*). By analogy with other enveloped viruses (*5*), this region in HIV-1 is probably not exposed until the viral and cell membranes are in close apposition. This implies the existence of a mechanism for exposure of the fusigenic domain at a step in virus infection subsequent to receptor binding. One such mechanism would be for the binding of CD4 to trigger a conformational change in gp120 that reveals the fusigenic domain. Here, we show that binding of purified recombinant soluble CD4 (sCD4) (*7*) or the purified V1 domain of sCD4 (*8*) to gp120 causes dissociation of the gp120-gp41 complex, which we suggest may be the initial stage in virus-cell fusion and cell-cell fusion.

To analyze the effect of sCD4 on virion-bound gp120, we devised a method (*9*) for the separation of virions from soluble gp120 and soluble core antigen p24 by gel-exclusion chromatography on Sephacryl S-1000 and for the detection of the viral antigens by enzyme-linked immunosorbent assay (ELISA) (*9, 10*) (Fig. 1). Conventional biochemical methods [for example, SDS–polyacrylamide gel electrophoresis and protein immunoblotting] were insufficiently sensitive for quantitation of the small amounts of HIV-1 antigens present in the maximum volume of viral culture supernatant (100 μl) that could be analyzed by chromatography under viral containment conditions. Preliminary experiments established that infectious HIV-1 was quantitatively eluted from the 2-ml column in or near the exclusion volume (0.6 to 1.2 ml), as expected for particles with a diameter of 100 to 150 nm (*11*) and a gel matrix with a particle exclusion limit of 300- to 400-nm diameter. In contrast, recombinant gp120 and p24 diluted in serum-containing culture medium were recovered quantitatively in broad peaks at an elution volume of 1.2 to 2.4 ml (*12*). The precision with which recovered viral antigens can be estimated is limited by the accuracy of ELISA measurements; in a typical experiment the recoveries (mean ± SD) from six separate chromatographic analyses of samples (50 μl) of the HIV-1 strain HTLV-III_{RF} incubated with and without sCD4 were 2.44 ± 0.22 ng of gp120 and 36.5 ± 4.6 ng of p24. Thus, we could cleanly separate virions (10^8 kD) from soluble viral antigens (10^4 to 10^5 kD) without

J. P. Moore, J. A. McKeating, R. A. Weiss, Chester Beatty Laboratories, The Institute of Cancer Research, London SW3 6JB, United Kingdom.
Q. J. Sattentau, Howard Hughes Medical Institute, College of Physicians and Surgeons of Columbia University, New York, NY 10032.

*To whom correspondence should be addressed.